Chapter 4
Magnetic Nanoparticles for Magnetic Resonance Imaging and Hyperthermia Applications

Emil Pollert, Graziella Goglio, Stéphane Mornet and Etienne Duguet

Abstract Medicine provides an increasing interest for magnetic nanoparticles, thanks not only to the growing control of their chemical and morphological design and colloidal stabilization, but also to the increasing tendency to use magnetic fields in diverse medical areas such as radiology, neurosurgery, or oncology. This contribution focuses on their potential usefulness as contrast agents for magnetic resonance imaging (MRI) and colloidal mediators for magnetic fluid hyperthermia (MFH). A physical background of these nanoparticles magnetism is first considered discussing their behavior either under static magnetic field or an alternating one. The design and preparation of magnetic fluids is then described from the synthesis of nanoparticles up to their colloidal stabilization in physiological media. Requirements with regard to in vivo administration are subsequently presented, i.e., the factors affecting their biocompatibility, their biodistribution, the solutions envisaged for enhancing their half-life in the blood compartment, and the active targeting of tumor cells. Finally, magnetic nanoparticles are considered as contrast agents for MRI and mediators for MFH, highlighting the involved problems and the current and future possibilities for solving them.

E. Pollert
Institute of Physics ASCR, Praha, Czech Republic

G. Goglio · S. Mornet · E. Duguet (✉)
CNRS, University of Bordeaux, ICMCB, Pessac, France
e-mail: duguet@icmcb-bordeaux.cnrs.fr

R. Brayner et al. (eds.), *Nanomaterials: A Danger or a Promise?*,
DOI: 10.1007/978-1-4471-4213-3_4,

4.1 Introduction

Magnetism and medicine have been sharing a fascinating common history for several centuries [1]. Some of the earlier applications of magnetic materials include removal of metallic objects from the bodies of animals and humans and the use of magnetite grains as antidote for the accidental swallowing of rust. In ayurvedic therapies, various kinds of iron oxides are still used as iron supplements for humans, especially children and pregnant women. More recently, miniaturization of electromagnets, development of superconducting electromagnets, and introduction of strong permanent magnets (Sm–Co and Nd–Fe–B) have stimulated the medical use of magnets in fields as diverse as radiology, dentistry, cardiology, neurosurgery, oncology, and immunoassays.

Moreover, well-calibrated magnetic nanoparticles (MNPs) in the size range 1–100 nm are currently produced in large quantities thanks to reproducible synthetic protocols. Several chemical routes allow modification of their surface for ensuring their colloidal stability in physiological media, protecting them from corrosion/dissolution, and making them less cytotoxic and derivatizable with biorelated molecules.

There are several reasons why MNPs are of particular interest in medicine. First, they are smaller than cells (10–100 m) and comparable to viruses (20–450 nm), proteins (5–50 nm), or genes (2 nm wide and 20–450 nm long). Therefore, they are able to circulate in the bloodstream (even in the thin lung capillaries), to cross-biological membranes, and to interact closely with biomolecules. Second, when their diameter is lower than about 10–15 nm, MNPs exhibit in the static regime at body temperature superparamagnetic behavior, i.e., without coercivity and remanent magnetization. Therefore, they are movable in magnetic field gradients and capable to create local magnetic fields. Consequently, they can be remotely manipulated in the "magnetically transparent" living tissues. Further, they may shorten the relaxation times of surrounding protons and generate heat due to magnetic losses when they are subjected to AC magnetic fields. Therefore, MNPs in a form of aqueous suspensions became recently inescapable tools for biologists, pharmacologists, and physicians. They are now routinely used as contrast agents in magnetic resonance imaging (MRI) and very soon clinical applications are expected in the field of cancer thermal treatment, namely magnetic fluid hyperthermia (MFH).

Even if some publications deal with oral MRI contrast agents for the gastrointestinal tract [2], the majority of published studies concern the intravenous administration route. The use of MNPs in the blood compartment depends on specific requirements concerning their plasma half-life and final biodistribution. The problem of the non-natural stealthiness of the nanoparticles toward the immune system, and the possibilities for resolving it, have been widely studied in the field of drug delivery from liposomes and polymeric nanoparticles [3]. Indeed, retention of drugs in circulation is a key step in the design of drug delivery carriers. The reason is obvious: even the most active compound in vitro is useless if in vivo it does not reside in the blood long enough to reach its target, while managing to

avoid, to some extent, premature metabolism, immunological reactions, toxicity, rapid excretion, and captation by undesired tissues [4]. Presently, many pieces of information are available concerning the immune system mechanisms, the factors affecting the biodistribution of nanoparticles, such as their size and shape, the hydrophobic/hydrophilic balance of their surface, their surface charge, and the solutions envisaged for targeting specific organs, tissues, or cells.

This review presents simultaneously the basic knowledge and an updated survey of the potential of MNPs for MRI and MFH applications through an understanding of the problems involved from the viewpoint of their overall requirements. One main intention of this contribution is to impart information about both the state of the art as well as the need for further progress and clinical development. Only typical examples among the most promising ones will be reported and discussed and a special emphasis will be made on cancer diagnosis and therapy. Only general references are provided for the reader to turn to for more information.

4.2 Magnetism of MNPs

4.2.1 Behavior in Static Magnetic Fields

4.2.1.1 Materials Magnetism Background

The magnetism of a solid is originated from the contributions of the constituting electrons, thanks to their quantum properties, that is, their spin angular moment and their orbital angular moment, which contribute to their magnetic moment. These electrons also determine the strength of the interaction between atoms in a solid, making the basis of the different macroscopic behaviors observed in nature. Massive materials can thus be classified into diamagnetic, paramagnetic, ferromagnetic, ferrimagnetic, and antiferromagnetic according to the arrangement of their magnetic dipoles in the absence and presence of an external magnetic field [5, 6].

If a magnetic material is placed in a magnetic field of strength H, the individual atomic moments in the material contribute to its overall response, the magnetic induction B:

$$B = \mu_0(H + M) \tag{4.1}$$

where μ_0 is the vacuum permeability, and the magnetization $M = m/V$ is the magnetic moment per unit volume, where m is the magnetic moment on a volume V of the material [7]. All materials are magnetic to some extent, with their response depending on their atomic structure and temperature. They may be conveniently classified in terms of their volumetric magnetic susceptibility χ, where

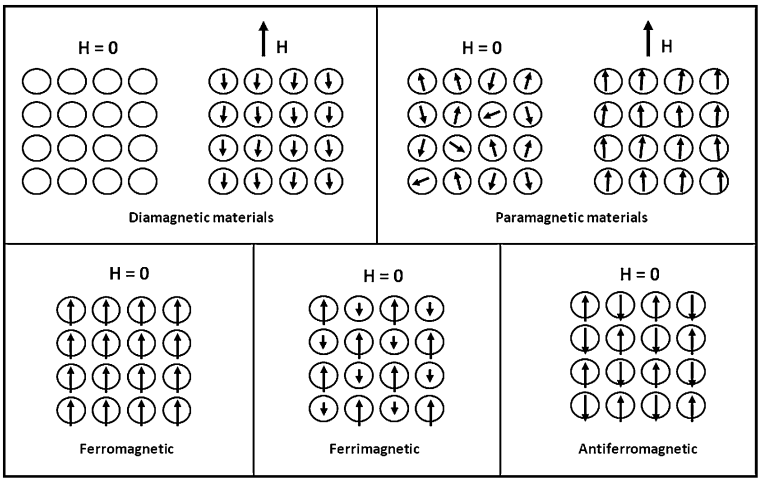

Fig. 4.1 Scheme illustrating the arrangements of magnetic dipoles for five different types of materials in the absence or presence of an external magnetic field (H). Redrawn from Ref. [8]

$$M = \chi H \tag{4.2}$$

describes the magnetization induced in a material by H.

Figure 4.1 shows schematic diagrams of these five different situations. If a material does not have magnetic dipoles in the absence of an external field and has weak induced dipoles in the presence of a field, the material is referred to as diamagnetic. The magnetization of a diamagnet responds in the opposite direction to the external field, within the range -10^{-6}–-10^{-3}. If a material has randomly oriented dipoles that can be aligned in an external field, it is paramagnetic. The magnetization of a paramagnet responds in the same direction as the external field ($10^{-6} < \chi < 10^{-1}$). The magnetic interactions derived from the above two types of materials are very weak because the thermal agitation at room temperature can make the magnetic moments to flip over continuously.

Some materials, however, exhibit ordered magnetic states and are magnetic even without an applied field. For a ferromagnetic material, the magnetic dipoles always exist in the absence and presence of an external field and exhibit long-range order (Fig. 4.1). Macroscopically, such a material displays a permanent magnetic moment and M is typically 10^4 times larger than it would appear otherwise. The difference in the source of the net magnetic moment can also be used to distinguish ferromagnetism from both ferrimagnetism and antiferromagnetism. In a ferrimagnetic material, there are always weaker magnetic dipoles aligned antiparallel to the adjacent, stronger dipoles in the absence of an external magnetic field. For an antiferromagnetic material, the adjacent dipoles are antiparallel in the absence of an external field and cancel each other.

That is why magnetic materials are referred to those characterized by either ferro- or ferrimagnetic features. Both ferro and ferrimagnetic materials can be

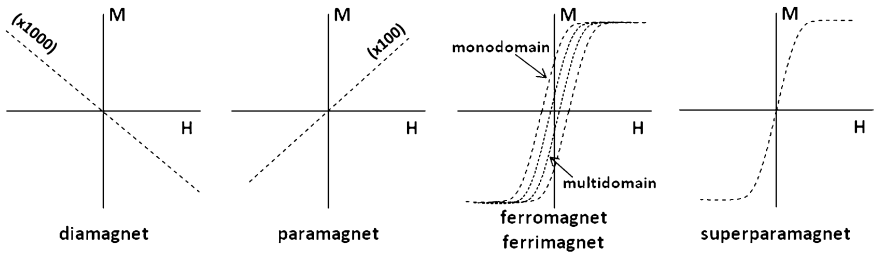

Fig. 4.2 Typical magnetization curves for the different types of magnetic materials

described using a number of basic parameters derived from the magnetization curve, where the magnetization M or flux density B is plotted against H (Fig. 4.2). Although a ferromagnetic material should have all its magnetic moments pointing in the same direction, a macroscopic piece of material cannot have this configuration because the amount of magnetostatic energy stored should be huge [9]. The way in which a solid can reduce this otherwise huge magnetostatic energy is to break itself up into regions called magnetic domains, or Weiss domains. Within a single domain, all magnetic moments remain parallel, but the individual domains are randomly oriented so that the net magnetic moment of the sample is nearly canceled (Fig. 4.3a). This situation generates interfaces between domains called domain walls or Bloch walls, where adjacent magnetic moments are in a nonfavorable configuration, so that these domain walls are highly energetic. Even though some energy is stored inside domain walls, the overall decrease in the total magnetic energy favors the multidomain configuration. Being formed by a competition between magnetostatic and exchange energies, domain walls have a finite width, determined by the ratio between these energies.

The susceptibility in ferro- and ferrimagnetic materials depends not only on temperature, but also on H, which gives rise to the characteristic sigmoidal shape of the magnetization curve (M–H curve), with M approaching a saturation value at large values of H (Fig. 4.2). Furthermore, one often sees hysteresis: it characterizes the irreversibility in the magnetization and demagnetization processes that are related to the pinning of magnetic domain walls at defects, dislocations, or vacancies within the material, as well as to intrinsic effects such as the magnetic anisotropy of the crystalline lattice. This gives rise to open M–H curves, called hysteresis loops. Actually, domain walls can move in response to an applied field: creation, growth, and extinction of domains can be induced by an external magnetic field because the external field imposes a preferred direction for the magnetic moments. For the spins in a given domain to change their orientation, it is required that the walls of that domain move. However, the magnetic field required to eliminate all domain walls (i.e., to align all magnetic moments in the same direction) has a definite value for a given sample, and is reproducible.

The saturation magnetization M_S (the maximum value of M), the remanence magnetization M_R (the residual magnetization at zero applied field strength), and

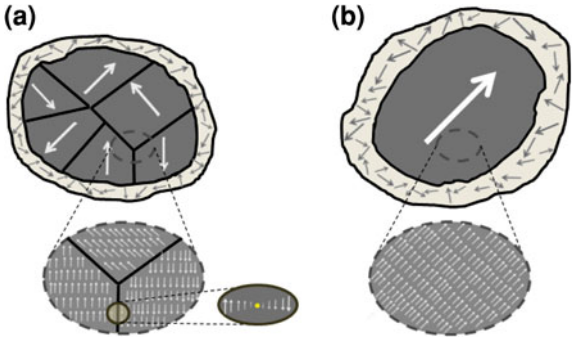

Fig. 4.3 **a** Schematic view of magnetic domains in a multidomain ferromagnetic particle having size larger than the critical diameter ($D > D_C$). For this particle, the whole material breaks down into randomly oriented magnetic regions. At the interface between domains, magnetic moments are twisted to fit the orientation at both sides of the domain walls. **b** Schematic view of a monodomain ferromagnetic particle having size smaller than the critical diameter ($D < D_C$). The spin disorder at the particle surface is represented by an annular region in both cases. Redrawn from Ref. [9]

the coercivity H_C (the external field required to reduce the magnetization back to zero) are deduced from the magnetization curve. A material is called a soft magnet if it can be magnetized readily in a weak field of $\sim$10 Oe (1 Oe = 1,000/4π Am^{-1}). On the other hand, hard magnets have very strong H_C and require large external fields applied in the opposite direction in order to be demagnetized.

Lastly, as the temperature increases, thermal motion competes with the tendency for the spins to align. When the temperature rises beyond a certain point, called the Curie temperature T_C, there is a second-order phase transition and the system can no longer maintain a spontaneous magnetization, although it still responds paramagnetically to an external field.

4.2.1.2 Magnetism of Nanoparticles

Magnetism is highly volume and temperature dependent because this property arises from the collective interaction of atomic magnetic dipoles [8]. When the size of a ferro- or ferrimagnet decreases to a certain critical value D_C, MNPs change from a state with multiple magnetic domains to one with a single domain (Fig. 4.3b). In that transition situation, H_C is maximal and the hysteresis loop is broad (Fig. 4.2). This critical size is achieved when the magnetostatic energy, which increases in proportion to the volume of the materials, becomes equal to the domain wall energy, which varies proportionally with the interfacial area between domains. For spherical and noninteracting MNPs, the critical size can be given as

$$D_C \approx \frac{18\sqrt{AK_{\text{eff}}}}{\mu_0 M_S^2} \tag{4.3}$$

where A is the exchange constant and K_{eff} is the effective anisotropy constant, i.e., a function of magnetocrystalline, shape and surface anisotropies. This critical size, which is generally of a few nanometers to a few tens of nanometers, varies from material to material.

The resulting magnetic behavior of an MNP with a size corresponding to a single magnetic domain depends on a competition between two energy contributions, i.e., on the terms $K_{\text{eff}}V$ and k_BT and the magnetic moment of the particle relaxes to its equilibrium position with a relaxation time τ_N given by the relation [10, 11]

$$\tau_N = \tau_0 \exp\left(\frac{K_{\text{eff}}V}{k_BT}\right) \tag{4.4}$$

where V is the particle volume, k_B is the Boltzman's constant, T is the absolute temperature, and τ_0 is a constant in the range of 10^{-9}–10^{-12} s.

Evidently due to a competition of the respective energetic contributions, two different situations have to be distinguished. Namely of $K_{\text{eff}}V \gg k_BT$, when the relaxation time $\tau_N \gg \tau_m$: the magnetic moment is stable and aligned parallel to the easy axis of magnetization and the MNP exhibits ferromagnetic or ferrimagnetic ordering. On the other hand, for a sufficiently small volume of the MNP, we have $k_BT \gg K_{\text{eff}}V$ and the relaxation time $\tau_N \ll \tau_m$. Then spontaneous fluctuations of the direction of magnetic moment between the two orientations along the (uniaxial) easy axis appear. It leads under an applied field to anhysteretic but still sigmoidal, M–H curves (Fig. 4.2) and the state of the system is called superparamagnetic.

The superparamagnetic state is displayed solely below the Curie temperature where the usual paramagnetic behavior starts. The border between the magnetically ordered and superparamagnetic state is, for a given particle volume, defined by the so-called blocking temperature T_B, evaluated from the zero field (ZFC) and field cooled experiments (FC) as the maximum in the temperature dependence of $d(\chi_\rho \text{ ZFC} - \chi_\rho FC)/\text{d}T$ [12].

4.2.1.3 Surface Effects

As the particles size decreases, a large percentage of all atoms in a nanoparticle are surface atoms, which implies that surface and interface effects become more important. Then an arising spin disorder and a reduced coordination of the broken exchange bonds lead to a spin-glass-like behavior of the surface spins or presence of canted spins on the outer surface layer of MNP (Fig. 4.3). Hence, a so-called magnetic dead layer arises and a decrease of the magnetization is observed. Another surface-driven effect is an enhancement of the magnetic anisotropy (K_{eff}) with decreasing particle size. Lastly, a magnetically inert surface coating, for example, silica or organic polymer, may modify the extent of the dipolar coupling between MNPs because its thickness controls the minimum distance between them. Overall, it must be concluded that the magnetic response of a system to an

inert coating is rather complex and system specific, so that no firm correlations can be established at present.

4.2.2 Behavior in AC Magnetic Fields

The situation in the static magnetic field, discussed in the preceding section, however changes under acting of an alternating field as it can be seen from the following relation deduced from the expression (4.4) for the relaxation time introduced above:

$$T_B = \frac{K_{\text{eff}} V}{C k_B} \tag{4.5}$$

The constant $C = ln(\tau_m/\tau_0)$ shows the sensitivity of the blocking temperature on the time window. It is equal to 27.6 for the DC measurements ($\tau_m = 100$ s) and decreases in the AC regime, e.g., down to the value of 10.8 for 480 kHz which is a frequency currently used in the magnetic fluid hyperthermia experiments. Therefore, the blocking temperature is shifted to higher temperatures and the field of the magnetically ordered state is extended in a corresponding way markedly towards higher temperatures. Evidently, it has an important influence on the magnetic losses decisive for the use of synthesized materials in magnetic fluid hyperthermia.

Returning to the hysteresis which gives rise to the open M–H curves seen for ferro- or ferrimagnets, it is clear that energy is needed to overcome the barrier to domain wall motion imposed by the intrinsic anisotropy and the pinning of magnetic domain walls in the material. This energy is delivered by the applied field and can be characterized by the area enclosed by the hysteresis loop. This leads to the concept that if a time-varying magnetic field is applied to a ferro- or ferrimagnetic material, one can establish a situation in which there is a constant flow of energy into that material, which is perforce transferred into thermal energy. A similar argument regarding energy transfer can be made for superparamagnets, where the energy is needed to coherently align the particle moments to achieve the saturated state [13].

4.2.2.1 Loss Mechanisms

Generally the power dissipation originating from the cyclic increase of internal energy produced by the magnetic work on the system is given by the relation

$$P = m_0 v \oint_H M \cdot \mathrm{d}H \tag{4.6}$$

where μ_0 is the permeability of free space and v the frequency of the AC field. Three different mechanisms can then be distinguished, namely hysteresis power losses, originating in the irreversibility of the magnetization process, Néel relaxation, conditioned by the rotation of the magnetic moments of the particles, and friction losses due to the Brownian rotation of the magnetic particles as a whole.

Hysteresis Losses

They are connected with the existence of irreversible magnetization loops and the power losses correspond to the relation derived from the general expression (4.6)

$$P = \mu_0 \pi \chi''(v) v H^2 \tag{4.7}$$

where χ'', the imaginary component of the susceptibility, is for polydisperse suspensions in a good approximation frequency-independent in the range of 100 kHz–1 MHz, currently used in MFH systems [14, 15].

Néel and Brownian Losses

Gradual decrease of the particle size leads to a transition to superparamagnetic state, where there is no more irreversible behavior characterized by the hysteresis loop and where the magnetic energy is converted to the thermal one by the rotation of the particle moment between two metastable antiparallel orientations, effectuated by two different ways, namely by the rotation of magnetic moments themselves (Néel rotation) and rotation of particles (Brownian rotation). The power dissipation can be described by similar functions as

$$P = \frac{\mu_0 \pi \chi_0 v^2 H^2 \tau_i}{[1 + (v \tau_i)^2]} \tag{4.8}$$

It is worth mentioning that the Néel relaxation time $\tau_i = \tau_N$ depends according to the relation (4.4) exponentially on the core volume (V), while the Brown relaxation time $\tau_i = \tau_B$ given by the relation (4.9)

$$\tau_B = \frac{3 \eta V_h}{kT} \tag{4.9}$$

involves the hydrodynamic volume of the particles (V_H) that may differ from that of the crystalline cores due to the presence of a stabilizing shell or due to agglomeration [16]. The resulting mean dependence of the corresponsive relaxation times is presented in Fig. 4.4. In realistic systems, the faster process dominates the overall remagnetization process, and for similar timescales, both mechanisms contribute as (4.10):

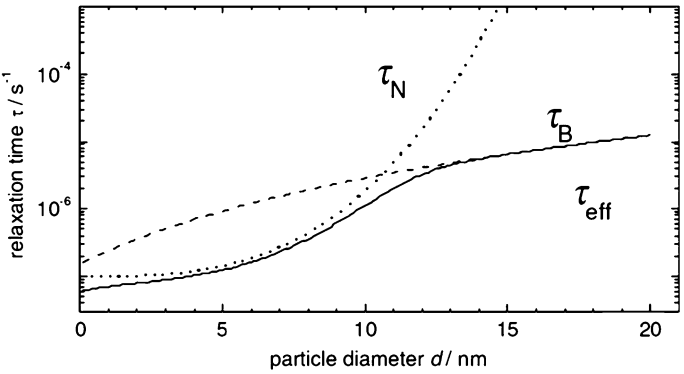

Fig. 4.4 Theoretical Néel (τ_N) and Brown (τ_B) relaxation times and effective relaxation time (τ_{eff}) for Fe_3O_4 magnetic nanoparticles versus particle diameter. Reprinted with permission from Ref. [16]. Copyright © 2007 Springer Science

$$\tau_{\text{eff}} = \frac{\tau_N \tau_B}{\tau_N + \tau_B} \tag{4.10}$$

It is then observed that below a critical size of the particles, the Néel loss mechanism is more effective while above this the Brownian loss mechanism plays a major role. Near to the critical size, both types of losses act equivalently.

The Brownian losses generally depend upon hydrodynamic size of the particles, but not on the size of the magnetic cores. Therefore, the type and thickness of coating over the magnetic materials can greatly influence heating. Lastly, in some situations, MFs based on ferro- and ferrimagnetic particles may also be concerned by Brownian losses.

4.2.2.2 Specific Absorption Rate

The heating ability of Magnetic Fluids (MFs) in the presence of AC magnetic fields can be estimated by colorimetric method and it is termed as specific absorption rate (SAR). SAR is estimated on the basis of direct observation of temperature rise and can be defined as the amount of heat generated in a second by one gram of magnetic element:

$$\text{SAR}_T = C \frac{m_S}{m_M} . \frac{\text{d}T}{\text{d}t} \tag{4.11}$$

where C is the specific heat capacity of the MF (or water in the case of diluted dispersions), dT/dt is the slope of temperature versus time graph at the considered temperature T, m_S is the mass of MF ,and m_M is the mass of the magnetic element in MF.

Concerning the electromagnetic devices used for colorimetry experiments, the technology of an AC magnetic field is still under development. Most experiments

were done with laboratory-made generators in the frequency range of 50 kHz to 1 MHz, with magnetic field amplitudes up to a few tens of kAm^{-1}. These parameters depended more on the technical availability of the generators used rather than on theoretical predictions for optimized SAR. Indeed, a frequency scan is technically tricky in this broad frequency range because of frequency-dependent skin effects and resistance of magnetic applicators. The majority of hyperthermia experiments were performed in an induction coil or in the air-gap of a magnetic inductor, cooled by water or air.

For clinical purposes, the heat generation, and hence, the SAR value is very crucial, the higher the value, the lower the injected dose. However, the SAR values measured by various scientists differed because of their strong dependence on factors such as the physical and chemical properties of the carrier fluid, the frequency and amplitude of the applied field, and the size, shape, surface coating, and chemical composition of the MNPs [17]. Therefore, in order to facilitate a comparison of various materials, two approaches were recently proposed and introduced.

The first approach is based on the use of the intrinsic loss parameter (ILP) independent of the frequency and amplitude of the AC magnetic field defined as

$$\mathrm{ILP} = \frac{\mathrm{SAR}}{H^2\, v} \tag{4.12}$$

Further, it is an effort to minimize the losses of heat arising due to the temperature gradient between the sample and its environment. Its elimination is achieved by a specific adiabatic shield heated continuously to the temperature equal to that of the sample [18, 19].

A simpler possibility to deal with the problem is based on the independent determination of the thermal losses [20] according to the relation

$$\mathrm{SAR}^{T}_{\mathrm{corr}} = \frac{1}{m_{\mathrm{magn}}}\left(-\frac{\mathrm{d}Q}{\mathrm{d}t}\right)^{T} + \mathrm{SAR}^{T}_{\mathrm{meas}} \tag{4.13}$$

where m_{magn} is the mass of the magnetically active matter and $\mathrm{d}Q/\mathrm{d}t$ are the thermal losses, i.e., the heat flow out of the sample. Nevertheless, let us note that the actual condition in the application of MFH may be even more complicated when the particles are placed in a moving medium, e.g., blood flow.

4.3 MF Design and Preparation

4.3.1 Synthesis of MNPs

MNPs can be synthesized by a wide variety of techniques ranging from mechanical (top-down approach) to chemical processes (bottom-up approach). For

in vivo applications, chemical processes are generally preferred, because they allow a better control of the purity, crystallinity, and size distribution. These processes include aqueous coprecipitation, thermal decomposition, sonochemistry, microemulsion, sol–gel, self-combustion, microwave refluxing, etc., for the synthesis of maghemite, magnetite, substituted iron oxides ($\gamma-M_xFe_{2-x}O_3$ or $M_xFe_{3-x}O_4$, where M = Al, Mn, Mg, Zn, Ni, Co, and Cu), metallic iron or cobalt and alloys such as FePt. For a detailed description of these synthetic routes, the reader will report on general review papers [8, 21–23] or review papers more specifically dedicated to iron oxide MNPs for biomedical applications [24–27].

These synthesis processes have their own benefits, but the achieved features of the MNPs depend strongly on the control of the experimental conditions. For instance, coprecipitation is a simple technique, but the type of salts (e.g., chlorides, sulfates, and nitrates), the cation oxidation states, the reaction temperature, the pH value, and ionic strength of the media greatly influence the size, shape, and composition of the final particles. Moreover, the morphology and size of the nanoparticles synthesized by thermal decomposition process greatly depend upon the ratios of the organometallic precursor, solvent, and surfactant, the temperature, and the reaction duration.

4.3.2 Colloidal Stabilization in Physiological Medium

Like other dispersions, aqueous MNPs dispersions are subjected to a number of destabilizing forces that can lead to phase separation due to flocculation and sedimentation [16].

One of the main causes of phase separation is the Van der Waals interactions between the high-surface particles that result in the formation of agglomerated material. In contrast to this, the sedimentation of single particles by gravitational force is prevented by thermal motion in the size range up to 20 nm. However, formation of small agglomerates due to the Van der Waals interactions significantly reduces thermal motion, and sedimentation may play an important role in the destabilization of a magnetic colloid.

In addition, the magnetic dipolar particles possess magnetic interactions that may be further enhanced by alignment of the dipoles in relation to their relative distance in outer magnetic field gradients [28]. Therefore, the colloids have to be stabilized against agglomeration by creating a protecting shell for each particle that prevents the particles from coming too close in contact with each other. This is possible using classical concepts from colloid chemistry, including electrostatic stabilization and steric stabilization.

As an example of electrostatically stabilized MFs, maghemite-based cationic fluids are easily prepared according to the method described by Massart [29]. In this process, magnetite nanoparticles are initially prepared by alkaline coprecipitation of iron (II) and iron (III) precursors in aqueous solution with an excess of concentrated ammonium hydroxide. Magnetite is oxidized into maghemite by heating in the

presence of HNO_3 and iron (III) nitrate. Maghemite particles are peptized in dilute HNO_3 solution to create positive surface charges on the particles. Washing and decantation with acetone using a magnet can remove the acidic precipitates. Simply by dispersing these particles into water produces aqueous MFs.

For in vivo applications, surface-charged nanoparticles are not advised and steric stabilization is generally preferred to electrostatic stabilization for physiological reasons (see Sect. 4.4.2). That is why the MFs are often prepared into aqueous solution of hydrophilic macromolecules or such macromolecules are grafted onto MNPs in a second step.

4.4 Size/Surface Requirements with Regard to i.v. Administration

4.4.1 Biocompatibility

Similar to other biomaterials, the biocompatibility of MNPs is assessed successively in vitro with animal or human cells, followed by in vivo tests with animals, before human clinical trials [30, 31].

For in vitro cytotoxic assays, the animal or human cells are generally grown on the culture plates. Well-grown cells are then treated with bare or surface-modified MNPs or MFs for several hours (up to 96 h). The effect of the nanoparticles on the cells is then estimated by the comparative study of treated and untreated cells (control) by visual counting of the viable cells. More sophisticated cell viability assays are generally performed. MTT assay is based on the reduction of the tetrazolium salt MTT (3-(4,5-dimethylthiazol-2-yl)-2,5-diphenyltetrazolium bromide) to formazan by succinate dehydrogenase. The formazan product is then quantified spectrofluorometrically, and hence, directly correlated to the activity of mitochondrial reductase enzymes. In sulforhodamine-B (SRB) assay, SRB binds to the basic amino acids of the cellular proteins. Thus, colorimetric measurement of the bound dye provides an estimate of the total protein mass that is related to the cell number. The distribution of MNPs on the cells can also be estimated by staining the treated or untreated cells with Pearl's Prussian blue (which stains mainly Fe^{3+}) or with Turnbull's reagent (which stains Fe^{2+} ions).

Animals such as mice, rabbits, dogs, and sheep are often chosen for experimental in vivo studies. The animals are grown under the prescribed guidelines of the animal ethics committee. The required dose of MF is then injected into the body of the animal and all the clinical changes are observed very carefully. For various time periods, blood samples are collected for hematological and serum biochemical analysis. During hematological analysis, the amount of hemoglobin, platelets, erythrocytes, leukocytes, neutrophils, lymphocytes, monocytes, basophiles, eosinophils, and hematocrit are generally compared with that of the untreated animal. In serum biochemical analysis, serum level of total protein,

bilirubin, albumin, glucose, cholesterol, alanine transaminase, aspartate transaminase, triglyceride, blood urea nitrogen, phosphorus, creatinine, calcium, and lactic acid dehydrogenase are compared with those of normal untreated animals.

It seems difficult to assert today which nanoparticles are toxic and which ones are not. MNPs absorption, distribution, metabolism, excretion, and toxicity depend on multiple factors derived from inherent physicochemical properties such as concentration, size, surface charge, nature of the surface chemical groups, and redox activity. First, the toxicity of particles that may dissolve in physiological conditions even at a very low rate has to be considered also from the viewpoint of the toxicity of the released metal cations. In such situations, endogenous chemical elements such as iron are preferred because the soluble iron becomes part of the normal iron pool (e.g., ferritin, hemosiderin, transferrin, hemoglobin). The lethal dose LD_{50} of pristine iron oxide nanoparticles is 300–600 mg_{Fe} per kilogram of body mass. A barrier coating may be engineered around each nanoparticle in the case of toxic metal elements. Second, in the case of insoluble particles, surfaces matter more than chemical composition, and efforts are in progress for embedding MNPs in biocompatible coating, often made of hydrophilic macromolecules and/or silica.

It is obvious that the MNPs toxicity is directly related to the concentration required for the diagnostic or therapeutic effect. Once the active targeting strategies (see Sect. 4.4.3) become efficient, and hence, allow concentrating MNPs essentially in the targeted organs, MNPs nontoxicity will become a less acute requirement [41].

4.4.2 Biodistribution and Passive Targeting Strategies

As soon as bare particles are, intentionally or otherwise, injected into the blood compartment, they are subjected to the action of the mononuclear phagocyte system (MPS) [32, 33]. It is defined as the cell family comprising bone marrow progenitors, blood monocytes, and tissue macrophages (such as Kupffer cells in liver). These macrophages are widely distributed and strategically placed in many tissues of the body to recognize and clear senescent cells, invading microorganisms or particles. The first step of the clearance mechanism is the opsonization process. Opsonins are circulating plasma proteins (various subclasses of immunoglobulins, complement proteins, fibronectin, etc.), that adsorb themselves spontaneously onto the surface of any invading entity. They are capable of interacting with the specialized plasma membrane receptors on monocytes and macrophages, thus promoting particle recognition by these cells. The second step consists of the endocytosis/phagocytosis of the particles by the circulating monocytes or the fixed macrophages, leading to their elimination from circulation and their simultaneous concentration in organs with high phagocytic activity. Therefore, after *i.v.* administration, particles are cleared up within minutes from the bloodstream; their typical final biodistribution is 80–90 % in the liver, 5–8 % in the spleen, and 1–2 % in the bone marrow [4]. Consequently, the remarkable

organization of the immune system is not compatible with long circulation times of any invading nanoparticle and MPS-mediated clearance is a major factor in determining their biodistribution. Nevertheless, it has provided an opportunity for the efficient delivery of therapeutic agents to these phagocytic cells, and therefore, to the related organs and more generally to any area where the macrophage activity is high, for example, infection/inflammation regions. Such an MPS-mediated targeting is called passive targeting.

If monocytes and macrophages are not the desired target, minimizing or delaying the nanoparticle uptake by the MPS is mandatory. The most satisfactory strategy consists of designing macrophage-evading nanoparticles (stealth nanoparticles) with plasma half-life as long as possible, in order to increase the probability to attain the desired target. The more efficient route is to prevent the opsonin adsorption and therefore to avoid the macrophage recognition. Among the physicochemical factors which are known to affect the opsonization process, the size, the surface charge density, and the hydrophilicity/hydrophobicity balance have been widely studied [32]. Therefore, the smaller the more neutral and the more hydrophilic the carrier surface the longer its plasma half-life.

In particular for hydrophobic particles, many studies concerned the development of core–corona structures where the corona is made of hydrophilic macromolecules for creating polymer brushes, acting as a steric surface barrier and reducing opsonin adsorption. Among the natural or artificial macromolecules, linear dextrans and derivatives are widely used. Other biological macromolecules have been investigated, for example, poly (sialic acid), heparin, and heparin-like polysaccharides complement regulatory proteins, etc., but because of their high cost and/or the possible immunological consequences associated with bacterial-made macromolecules, efforts have been directed to design synthetic hydrophilic macromolecules. In particular, great efforts have dealt with the covalent anchorage of poly (ethylene glycol) (PEG) macromolecules onto the particle surface. This process is so widely used that it is called 'PEGylation.' In fact, PEG is a flexible polyether, hydrophilic (but also soluble in some organic media), not biodegradable, but easily excreted from living organisms. Its functional end-groups are available for derivatization leading to numerous routes for covalent attachment onto preformed functional surfaces or anchoring during the synthesis of particles. PEG has been shown to be the most effective polymer for suppressing protein adsorption, the optimal molecular weight varying between 2,000 and 5,000 $g.mol^{-1}$ [32]. These values are still in debate, and in particular, the surface density appears to be as important as the molecular weight [33].

An escape of the macrophage-evading particles from the circulation is normally restricted to sites where the capillaries have opened fenestrations as in the sinus endothelium of the liver or when the integrity of the endothelial barrier is perturbed by inflammatory processes (e.g., rheumatoid arthritis, infarction, infections) or by some types of tumors. Therefore, the idea of exploiting such vascular abnormalities for extravasating and accumulating nanoparticles in these inflammatory sites or tumors is also particularly attractive. This strategy is also considered as a passive targeting one, but independently of the MPS mediation.

4.4.3 Active Targeting Strategies

In order to increase the probability to redirect long-circulating particles to the desired target, their surface has to be labeled with ligands that specifically bind to surface epitopes or receptors on the target sites (molecular recognition processes such as antibody–antigen interactions). Such a strategy should open the possibility of targeting specific cell types or subsets of cells within the vasculature and even elements of vascular emboli and thrombi [33–36]. In the case of cancer therapy, active targeting could allow the selective destruction of the cancer cells, even if they have escaped the tumor mass and disseminated as metastatic cells. These ligands must be coupled to the surface of stealth carriers. They include oligosaccharides, oligopeptides, folic acid, antibodies, and their fragments. As an example of tumor targeting, folic acid (vitamin B essential for cell division processes) may be used to take advantage of the frequent overexpression of folate receptors onto the surface of human cancer cells [37].

4.4.4 Surface Activation and Bioconjugation

In particular for the active targeting purpose, the surface of MNPs shall be derivatized. The process of proper linkage of biomolecules with nanoparticles under mild conditions is commonly called bioconjugation. Two main approaches to attach biomolecules on the surface of MNPs are physisorption and chemisorption. In physisorption, biomolecules directly attach to the surface of particles owing to weak interaction (electrostatic or Van der Waals forces), whereas, in chemisorption, biomolecules attach by the formation of covalent chemical bonds.

Oxide or metal nanoparticles themselves may not be capable of covalent attachment to biomolecules owing to their poor surface chemical reactivity. Hence, surface activation is required to create the chemical functions needed for coupling biomolecules to MNPs. The direct surface modification of metal oxides generally uses carboxylic acids, alkyltrialkoxysilanes, or alkyl phosphonates. Reactive function such as amino, thiol, aldehyde, or carboxylic group are generally present on the alkyl fragment and become the main surface groups. A coupling agent is generally required for linking this surface function with biomolecules (Table 4.1).

In numerous situations, the direct coupling with the inorganic surface is not preferred and one alternative strategy consists in taking advantage of the intrinsic reactivity of the hydrophilic macromolecules used for embedding and sterically stabilizing MNPs.

Table 4.1 Non-exhaustive list of coupling strategies of biomolecules on the activated surface of MNPs

Surface reactive function available on MNPs	Reactive function available on biomolecules	Possible coupling agent
-COOH	$-NH_2$	sulfo-N-hydroxysuccimide
$-NH_2$	-COOH	sulfo-N-hydroxysuccimide
$-NH_2$	$-NH_2$	glutaraldehyde
$-NH_2$	-SH	sulfo-SMCC[a]
-SH	$-NH_2$	sulfo-SMCC[a]
-OH	$-NH_2$	carbonyl diimidazole

[a] *SMCC* succinimidyl 4-(N-maleimidomethyl)cyclohexane-1-carboxylate

4.5 MNPs as Contrast Agents for MRI

4.5.1 MRI Background

Medical applications of MRI have steadily widened over the past decade and MRI is now one of the preferred cross-sectional imaging modalities [7, 38]. The principle of MRI is based on the behavior of the hydrogen protons present in a tissue under an applied transverse radiofrequency pulse perturbing their spins from the ordered, aligned state established initially by the applied magnetic field, B_0. The subsequent return of the spins to the original state is denoted as the relaxation phenomenon. In fact, it consists of two independent processes, namely longitudinal relaxation which is the return of longitudinal magnetization in alignment with B_0 and is termed T_1-recovery and transverse relaxation which is the vanishing of transverse magnetization and is termed T_2-decay. As a time constant, T_1 is the time which is required for 63 % of the longitudinal magnetization to recover in the tissue. In contrast, T_2 decay is not a process of dissipation or absorption of energy into tissue. During the *rf*-pulse, hydrogen nuclei are spinning in phase with each other. After the *rf*-pulse, the magnetic fields of all the nuclei interact with each other; energy is exchanged between those nuclei. The nuclei lose their phase coherence and spins become arranged randomly. Time constant T_2 is the time which is required to decrease the transverse magnetization to 37 % of its initial value.

In order to correlate the signal to its spatial origin, at least one of the two fields (i.e., B_0 or the *rf*-field) has to vary over space. Relaxation data are collected by a computer which applies a two-dimensional (2D) Fourier transform to give the amplitudes of NMR signals and permits reconstruction of the 3D images. Thanks to sequence parameters such as the repetition time *TR* (elapsed time between successive *rf*-excitation pulses) and the delay time *TE* (time interval between the *rf*-pulse and the measurement of the first signal), the operator obtains the desired type of image contrast. Basically, short *TRs* increase T_1 effects, whereas long *TRs* allow tissues to reach complete longitudinal magnetization, reducing T_1 effects. Short *TEs* minimize T_2 effects of tissues, whereas long *TEs* allow the loss of

transverse signal, enhancing T_2 effects. Therefore, T_1-weighted imaging is obtained by utilizing a short *TR* and a short *TE*, allowing full recovery of tissues with a short T_1 (e.g., fat) while allowing only partial recovery of tissues with long T_1 (e.g., cerebrospinal fluid). On the other hand, for T_2-weighted imaging, long *TRs* and long *TEs* are used. Fluids have a very long T_2 and they are frequently associated with pathologies (e.g., internal injuries, cancer lesions), so T_2-weigted images are generally preferred for such diagnostics.

4.5.2 MR Contrast Agents

In actual practice, tissues may be differentiated on MR images because T_1 and T_2 depend on proton environment. However, in many clinical situations, these intrinsic differences are small and exogenous contrast media are sometimes required for a better delineation of tissues. An ability to increase the relaxation rates of surrounding proton spins is called relaxivity $r_{1,\,2}$ and defined as:

$$\left(1/T_{1,2}\right)_{\text{in presence of contrast agent}} = \left(1/T_{1,2}\right)_{\text{without contrast agent}} + r_{1,2}[\text{contrast agent}]$$

where *[contrast agent]* is the contrast agent concentration in millimolars.

The first generation of these contrast agents consisted of high spin paramagnetic ions, usually Gd^{3+} in very stable nontoxic chelate form obtained through complexation by low molecular weight chelating molecules, such as diethylenetriaminepentaacetic acid [39]. Gd-chelates have an extracellular distribution before their excretion by the kidneys. Hydrogen atoms of water in proximity to such chelates experience a faster T_1-relaxation ($r_1 = 3.7\ \text{mM}^{-1}\text{s}^{-1}$). Consequently, differences in agent concentration result in contrast enhancement on T_1-weighted images ('positive' contrast). They have to be administered in concentrations of about 0.1 mmol per kilogram of body mass to produce visible effects on the images. Gd-chelates are routinely used for distribution into the intravascular and interstitial space to enhance signal of fluid compartments or lesions (renal function, status of the blood–brain barrier, etc.). Their main disadvantages are their short plasma half-life and their relatively low relaxivity.

Superparamagnetic MNPs have also been developed as MR contrast agents because of their larger magnetic moment in the presence of B_0 (susceptibility agents) [2, 40]. Therefore, their relaxivity is significantly higher ($r_1 = 10$–$15\ \text{mM}^{-1}\text{s}^{-1}$ and $r_2 = 40$–$190\ \text{mM}^{-1}\text{s}^{-1}$) than that of Gd-chelates. In most situations, they are used for their significant capacity to produce predominantly T_2 relaxation effects, which result in signal reduction on T_2-weighted images ('negative' contrast). Basically, the phenomenon may be described by the large magnetic field heterogeneity around the nanoparticle through which water molecules diffuse. This predominant effect on the T_2 relaxation time does not prevent their use on the T_1 relaxation time on the condition of low concentrations and appropriate imaging sequences.

This new generation of contrast agents is often called (U)SPIO for (Ultrasmall) SuperParamagnetic Iron Oxide. They consist of nonstoichiometric iron oxide cores (3–10 nm in diameter) whose chemical composition varies continuously from Fe_3O_4 to γ-Fe_2O_3. For *i.v.* administration, they are generally synthesized in a one-step process by alkaline coprecipitation or iron (II) and iron (III) precursors in aqueous solutions of hydrophilic macromolecules, essentially dextran or carboxy-dextran. The role of this macromolecular corona is the limitation of the magnetic core growth during the synthesis, their steric stabilization in water (and later in physiological medium) and in vivo the reduction of the opsonization process. Interactions between magnetic cores and macromolecules are weak (essentially Van der Waals and hydrogen interactions) and generally prevent any efficient derivatization of dextran corona without macromolecule depletion.

(U)SPIO pharmacokinetics, biodistribution, and toxicity properties were studied and allowed to define the potential uses of these contrast agents. The lethal dose LD_{50} of a dextran–iron oxide complex was found to be 2,000–6,000 mg_{Fe} per kilogram of body mass, whereas it is 300–600 mg_{Fe} per kilogram for pristine iron oxide. (U)SPIO have in common their specific uptake by the MPS, explaining why, if they are not entirely captured by the liver and the spleen, they are currently widely evaluated as MRI contrast agents for the diagnosis of inflammatory and degenerative disorders associated with a high macrophage phagocytic activity. The nanoparticles are metabolized in lysosomes and it may be noticed that the iron load resulting from administration of the clinical dose ($\sim$1 mg_{Fe} per kilogram of body) is low compared with the total store in the human body (about 3,500 mg).

4.5.3 Liver MR Imaging

SPIO, with a hydrodynamic diameter over 50 nm (up to 150 nm), are efficiently accumulated in MPS-organs ($\sim$80 % of the injected dose in liver and 5–10 % in the spleen with plasma half-life lower than 10 min.). Therefore, SPIO decrease liver and spleen signal within several minutes after *i.v.* administration. Malignant tumors or metastases as small as 2–3 mm, which are typically devoid of a substantial number of phagocytic Kupffer cells, appear as hyperintense (bright) lesions contrasted against the hypointense (black) liver on T_2-weighted sequences. The first SPIO, Endorem® (Guerbet, France), was marketed in Europe more than 15 years ago.

4.5.4 Metastatic Lymph Node MR Imaging (MR Lymphography)

Nodal disease is an independent adverse prognostic factor in many types of cancer. Thanks to their smaller size (lower than 40 nm) and the hydrophilicity of their

dextran corona, USPIO may act as stealth particles; their plasma half-life is higher than 20 h and some particles leak to the interstitium, where they are cleared by the macrophages of the lymphatic system or drained via the lymphatic system and subsequently accumulated in the lymph nodes. Hence, they allow diagnosing hyperplastic and tumorous lymph node by MR lymphography. A decrease in signal intensity indicates active uptake of particles into macrophages in normally functioning nodes, whereas metastatic nodes remain isointense with the precontrast image (Fig. 4.5). Clinical trials have reached phase III using Sinerem® (Guerbet, France) for the detection of lymph node metastases (head and neck and pelvis regions) [2].

4.5.5 Further Clinical Applications in Progress

Because USPIO are taken up by the liver and spleen more slowly than SPIO, they remain in the blood circulation for a longer time. On the other hand, USPIO have a more favorable T_1/T_2 ratio that facilitates T_1-weighted MR techniques at low B_0 (lower than 0.5 T). Thus, USPIO significantly shorten the T_1 of blood during the first hours after *i.v.* injection and may be used as T_1-agent. Thanks to these combined features, Sinerem® has been developed as MR blood pool agents for indications such as evaluation of cerebral perfusion, myocardial or renal perfusion, angiography or detection of hepatic vascular lesions [2].

Animal experiments and clinical studies are currently dedicated to USPIO-tagged macrophage imaging in several inflammatory and degenerative diseases. This modality could be used not only primarily for disease detection, but also for prediction and follow-up of the therapeutic efficacy [2]. Encouraging results were obtained in the case of cerebral ischemic lesions and brain inflammations, atheromatous plaques prone to rupture, multiple sclerosis, kidney disease, arthritis, infection caused by Staphylococcus aureus, and kidney and cardiac graft rejection. Moreover, USPIO are now reputed to be useful to evaluate (i) areas of blood–brain barrier dysfunction related to tumors and other neuroinflammatory pathologies, (ii) the cerebrovasculature using perfusion-weighted MRI sequences, and (iii) in vivo cellular tracking in central nervous system disease or injury [43].

Molecular MR imaging is one of the main MRI developments in progress, because clinicians dream about a contrast agent that would accumulate highly and specifically in malignant tumors, allowing an accurate diagnosis at a stage when the disease would be still treatable. Such tools would also be of a great interest for cardiovascular, inflammatory, and degenerative diseases. It concerns tissue-specific MR contrast agents [39, 44, 45]. Ligand-labeled (U)SPIO were designed (e.g., human polyclonal IgG, anti carcinoembryonic antigen, anti-glioma, L6 antibody, anti-epidermal growth factor receptor) and investigations carried out in small animals revealed the possibility to achieve a distinct concentration of the magnetic label at the target. However, the required dose of the labeled antibody is still too high to make a commercial development realistic. That is why the use of small

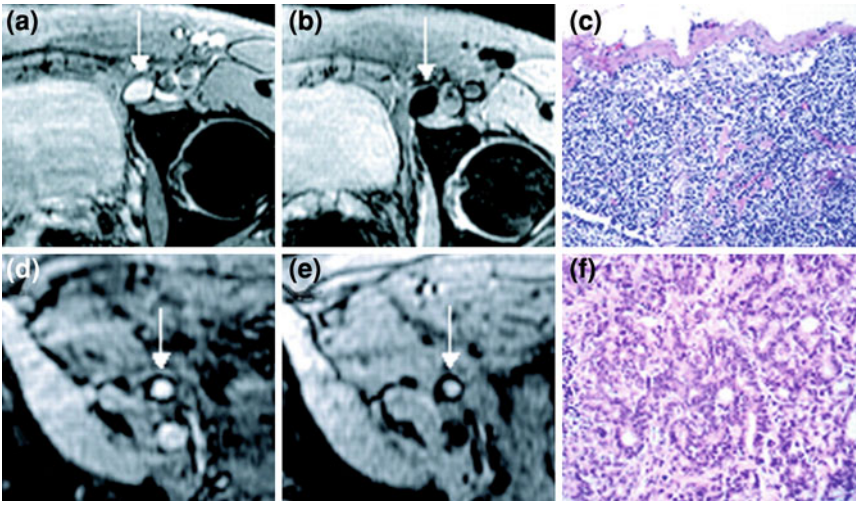

Fig. 4.5 Magnetic resonance imaging nodal abnormalities in two patients with prostate cancer. As compared with conventional MRI (Panel **A**), MRI obtained 24 h after the administration of USPIO (Panel **B**) shows a homogeneous decrease in signal intensity due to the accumulation of lymphotropic superparamagnetic nanoparticles in a normal lymph node in the left iliac region (*arrow*). Panel **C** shows the corresponding histologic findings (hematoxylin and eosin, x125). Conventional MRI shows high signal intensity in an unenlarged iliac lymph node completely replaced by tumor (*arrow* in Panel **D**). Nodal signal intensity remains high (arrow in Panel **E**). Panel **F** shows the corresponding histologic findings (hematoxylin and eosin, x200). Reprinted with permission from Ref. [42]. Copyright © 2003 Massachusetts Medical Society. All rights reserved

ligands, in particular, folate-mediation, appears more realistic for tumor MRI diagnostic. Lastly, spatial resolution is the key parameter for the detection of low concentrations of ligand-labeled (U)SPIO and the development of high magnetic field (up to 7 T) would allow achieving a high spatial resolution while maintaining a satisfactory signal-to-noise ratio.

The development of stem cell-based therapies requires quantitative and qualitative assessment of stem cell distribution to target organs (in the case of systemic administration), differentiation outcome, and engraftment. If labeled with MR contrast agents, they could be visualized and tracked by MR imaging. In the reported experiments, stem cells are generally labeled in vivo by using eventually a transfection agent (e.g., protamine sulfate, polylysine, cationic liposome, or cationic dendrimers) for USPIO, which are less efficiently internalized than larger SPIO. Labeled cells showed a gradual decline of intracellular iron oxide particles with increasing time after incubation. This effect can be attributed to cell division and exocytosis or release of iron from nonviable cells. Several experiments on animal models were reported and recently reviewed [2].

4.5.6 Next Developments

Even if (U)SPIO contrast agents are now routinely used in hospitals, no precise structure/activity relationship has been described to fully predict their stability, as well as their pharmacokinetics and safety [25]. An extended physicochemical characterization is required but remains difficult owing to their small dimensions, reaching the analytical resolution limits of many commercial instruments.

In addition to the clinical developments presented in the previous sections, current efforts are concerning the improvement of the (U)SPIO platforms. In particular, their chemical stability is insufficient, if dextran macromolecules must be derivatized for bioconjugation (see Sects. 4.5.2 and 4.5.5). Improvement may be achieved when dextran macromolecules are cross-linked in a second step for enhancing the mechanical entrapment of magnetic cores [46] or when they are chemically bonded to the magnetic cores through the use of coupling agents [47].

In order to improve the MR contrast and/or decrease the magnetic core size, metal MNPs are currently investigated. Indeed, because of their higher saturation magnetization, larger effects on proton relaxation are expected. Moreover, below $\sim$8 nm, inorganic nanoparticles can be readily excreted from the body by renal clearance [48]. For instance, cobalt, iron or FePt MNPs were recently obtained and evaluated as T_1 or T_2 contrast agents. Preliminary results were promising, nevertheless, chemical stability against oxidation, surface chemistry for bioconjugation, and toxicity/pharmacokinetics concerns shall be reconsidered in comparison to the now well-known (U)SPIO. Enhanced MRI sensitivity was also achieved with $MnFe_2O_4$ MNPs that displayed the highest magnetic susceptibility and the strongest r_2 relaxivity value of 358 $mM^{-1}s^{-1}$ (to compare to 40–190 $mM^{-1}s^{-1}$ for conventional (U)SPIO). They would enable the MR detection of tumors as small as 50 mg ($2 \times 5 \times 5$ mm^3). More recently, thermal decomposition method allowed to prepare a series of 15 nm sized Zn^{2+} doped nanoparticles of $(Zn_xMn_{1-x})Fe_2O_4$ [49]. It was shown that for $x = 0.4$ the r_2 value of ferrite was 13.8 and 7.8 times larger than those of conventional iron oxide-based contrast agents, respectively.

Lastly, a significant development for the future of magnetic imaging in the human body concerns a new imaging modality, magnetic particle imaging (MPI), initially developed by Philips Research [48]. The technique takes advantage of the nonlinear magnetization curve of small magnetic particles to generate harmonic responses to time-varying fields that can be detected using standard lock-in methods to a high degree of precision, and with a very low background signal to contend with. The imaging capability is the result of the following concept: in the presence of a large enough DC magnetic field, the magnetization curve is flat, and as such, the harmonic signals disappear. The corollary of this is that if one applies a DC field to all but a small 'field-free point' on the sample, the only harmonic signal received comes from that field-free point, and all other signals are damped out. MPI has great potential for medical applications such as vascular or small intestine imaging, where fast dynamic information is required, and the targets are

located relatively deep below the skin, the latter because the MPI signal is virtually unattenuated by intervening tissue.

4.6 MNPs as Mediators for Magnetic Hyperthermia

4.6.1 Hyperthermia Modalities

The choice of therapies against cancer such as surgery, radiation therapy, chemotherapy, hormone therapy, or biological therapy depends to a great extent upon the type and location of the cancer, the stage of the disease, age, and general health of the patient. Each has its own limitations, as they cause severe side effects to the surrounding tissues in the case of the localized therapy and to the whole body in the case of systemic therapy. Heat can be applied locally or to the whole body according to the requirements and exhibit low side effects. Further, both in vitro and in vivo studies and clinical experiments showed improved results when hyperthermia is applied in combination with other therapies such as chemo or radiotherapy [50].

As the name indicates, the hyperthermia treatment is generally carried out in the temperature range of 42–46 °C, which is above physiological growth temperature (for humans, it is above 37 °C). This is termed as mild hyperthermia. In this temperature range, tumor hypoxic (poorly oxygenated) cells are more heat-sensitive compared to the normal euoxic (well oxygenated) cells. Hence, the normal cells survive, while the cancerous cells get killed; this creates an interesting way for the therapy of cancer with minimal side effects. In addition, the cancerous tissues have inadequate blood supply, and thus, are not able to dissipate heat energy at the same rate as that of normal ones. Hyperthermia is applied sometimes above 46 °C and it is termed as thermoablation. The effect of hyperthermia exclusively depends upon the treatment temperature and on the exposure time at that temperature. Interestingly, it has been observed that a temperature decrease of 1 °C in the temperature range of 42.5–47 °C required doubling of the exposition time, whereas below 42.5 °C, the heat exposure time has to be prolonged by four times to get the same effect.

Hyperthermia during in vitro studies can cause several morphological changes in the cells and can detach them from the culture flask and finally kill them [51]. The mechanism of heat-induced cell death causes numerous cellular changes such as in the cell membrane, pH, nuclear and cytoskeleton structures, cellular metabolism, macromolecular synthesis, intracellular signal transduction in hormone-receptor interactions, expression of the heat shock proteins, chromatin organization, and synthesis of DNA and RNA. The degeneration of mitochondria, enzymes, and various kinds of proteins also get induced by hyperthermia.

The cell death due to hyperthermia could be classified either by apoptosis or necrosis. Apoptosis is an orderly process of programmed cell death and can be

characterized by distinct morphological features such as nuclear condensation, membrane blebbing, blisters, and echinoid. On the other hand, thermoablation treatment induces necrotic cell death, which is a pathologic phenomenon; it usually occurs when the cells find it difficult to survive following a major external damage. Necrotic cells have swollen nuclei without chromatin condensation, and can be characterized by a gradual dissolution of cell structure and lysis of the plasma membrane.

The selection of hyperthermia modalities that can be applied locally or to the whole body generally depends upon the heating source and on the types of cancer. On the basis of types of heating source, it can be divided into three groups, namely, heat applied from external source (e.g., hot bath, air, wax, blanket), contactless sources (e.g., radiofrequency, ultrasound, microwave, and infrared devices), and heat source inserted into body (e.g., probes, antenna, laser fibers, and mediators) [47].

The advanced hyperthermia devices such as ultrasound or electromagnetic radiation have their own limitations as the heat energy generated by them cannot be delivered to deeply situated cancer tissues without destroying the surrounding normal one. However, this could be overcome by inserting the heating source mediators inside the body where the electromagnetic energy applied on these deep situated mediators by an external electrical or magnetic field gets transformed into heat.

The inserted mediators can be either of macro, micro or nanometric size and they can be stimulated either by capacitive applicators using the electrical component of electromagnetic fields (*E*-field), or by inductive applicators using magnetic component (*H*-field). Macroscopic mediators must be inserted within the body by surgical intervention, whereas micro or nanoscale mediators can be injected as particle dispersion. However, during capacitive heating, *E*-field may cause heating of the surrounding tissues due to their conducting nature (eddy currents). Further, the difference in the dielectric permeabilities of different tissues leads to inhomogeneous temperature rise. On the other hand, in inductive mediator heating, this problem could be overcome as body tissues do not produce any heat in the presence of AC magnetic field. However, to suppress the effect of *E*-field completely, the optimized value of the product of $H \times f$ (where H is the amplitude and f the frequency of the AC magnetic field) is restricted to 4.85×10^8 $\mathrm{Am^{-1}s^{-1}}$ for a patient treated for one hour [17]. Depending on the diameter of the exposed body region, on the duration of the treatment, and on the seriousness of the illness, this critical product may be exceeded. Moreover, to avoid neuromuscular electrostimulation, f should be higher than 50 kHz, and it should be lower than 10 MHz for appropriate penetration of the *rf*-field.

4.6.2 Magnetic Fluid Hyperthermia

Even by stressful intervention, the macroscopic inductive heating mediators such as ferromagnetic rods or seeds (1 mm diameter and 1–7 cm of length) cannot be accessible to all tumors. Nevertheless, lack of uniform temperature may also cause

potential thermal underdosage to some critical regions. Hence, the magnetic fluid hyperthermia (MFH), in which colloidal dispersion of inductive heating mediators of micro or nanoscale is used, appears as the most promising therapy. In this case, the particles could be homogeneously distributed due to their ultramicron size, and hence, could produce uniform temperature all around the tissue. It has already been discussed that the cells uptake MNPs by endocytosis and the uptake by the cancerous tissue is even higher owing to their leaky vasculature, which is further helpful during cancer therapy. There is the benefit of stable deposits of MNPs surrounding the tumor tissues in the sense that once the particles are applied, then repeated thermotherapy can be performed without any further addition of particles. Even the daughter cells from a particle containing parent cell should contain up to 50 % of the particle amount of the parent cell, and thus, the descendants would still be cured by future MFH sessions.

The concept of using magnetic hyperthermia as cancer therapy was initiated by Gilchrist and coll. in the late fifties [52]. After a considerable gap, investigations were renewed in vitro, and now, in vivo. The first studies used magnetite nanoparticles surrounded by a dextran corona similar to the (U)SPIO contrast agents developed for MRI. In vitro experiments showed that these nanoparticles were internalized by cancer cells. Applying an alternating magnetic field (520 kHz, 7–13 kAm^{-1}) caused the tumor to diminish in the same way as it would in a bath of hot water. Subsequently, dextran was abandoned because it would appear to degrade too soon. It was then shown that direct injection of particles into the tumor has an advantage (still not fully understood) called the thermal bystander effect: even though the particles are concentrated at the deposition points before applying the alternating magnetic field, they distribute themselves much more uniformly after the first application of the AC magnetic field [53].

Jordan, Maier-Hauff and their collaborators at Clinique Charité in Berlin are now the most famous clinical research team, because they developed a full-sized human magnetic field applicator (MFHW 300 F, Hyperthermiesystem GmbH, Berlin at a frequency: 100 kHz, variable field strength: 2.5–18 kAm^{-1}) and a biocompatible MF made now of surface-aminated magnetite nanoparticles (MagForce Applications GmBH, Berlin, and MagForce Nanotechnologies AG, Berlin, Germany). They performed the first-ever clinical studies based on MFH [54]. The MNPs dispersion is injected within the tumor under general anesthesia. To solve the problem of the temperature distribution, numerical simulations based on tomographic images of the tumor allow optimizing the position of the MNPs deposits (Fig. 4.6). The expected heat distribution within the tumor is estimated by the Nano-PlanW software planning system (MagForce Nanotechnologies AG, Berlin, Germany).

Phase I clinical trials (feasibility studies) were performed to patients having prostate carcinoma [56], as well as glioblastoma multiforme [57]. This last study involved 14 patients receiving treatment via a combination of fractionated external beam radiotherapy and several sessions of thermotherapy. Aminated-MNPs were injected into multiple sites throughout each tumor. The choice of injection sites was based on data from a comprehensive series of MRI scans of the cranium

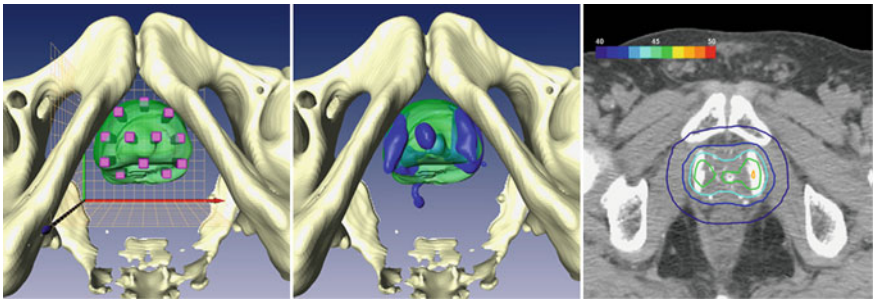

Fig. 4.6 *Left* Tomography of a prostate (*green region*), indicating the path of needles used to deposit 0.5–1 mL (per path) of the particle dispersion. *Center* Tomography after injecting the nanoparticles (*blue*). *Right* Image showing the nanoparticle deposits (*white* because denser than the prostate tissue) and calculated isotherms. Reprinted with permission from Ref. [55]. Copyright © 2007 Elsevier

coupled with the NanoPlanW software. The iron oxide nanoparticles (core size 15 nm) were dispersed in water at a concentration of 112 $mg_{Fe}mL^{-1}$. Each tumor was injected with 0.1–0.7 mL of the MF per milliliter of tumor and then exposed to a magnetic field of 3.8–13.5 kAm^{-1} alternating at 100 kHz. The study successfully demonstrated that this form of thermotherapy using MNPs could be safely applied to the treatment of brain tumors and that hyperthermic temperatures could be achieved. Follow-up computed tomography scans and reproducible temperature measurements confirmed that these deposits were stable over several weeks. Patient survival and local tumor control were not considered primary endpoints of this study; however, clinical outcomes were observed to be promising with the therapy being well tolerated by all patients. More complete evaluation of clinical outcomes is to be assessed in a phase II study (efficacy study) on 65 patients with recurrent glioblastoma multiform. Phase I clinical trials concerning pancreatic and esophageal cancers and local recurrences of residual tumors (e.g., cervical and prostate cancers, sarcomas) are also in progress.

The rather long period of gestation from first in vitro studies to eventual clinical application reflects the considerable technological and regulatory difficulties to be overcome in any attempt to develop a clinically acceptable and useful therapy of this type [48]. It is not merely enough to develop MNPs that heat upon exposure to an AC magnetic field, although that is clearly an important prerequisite. It is also important to know how to appropriately administer sufficient amounts of the particles to the intended target tissue and to be able to generate enough heat from them by exposure to a tolerable level of AC magnetic field that does not itself cause any undesirable side effects. The methodology developed by the MagForce group seems to successfully address each of these issues.

4.6.3 Next Developments

It is clear that if magnetically induced hyperthermia is to achieve the desired results, a certain number of aspects need to be improved. This includes not only the synthesis and properties of the MNPs-based mediators but also a better understanding of the physics involved in the loss phenomena, modeling of the in vivo temperature distribution, and development of a safe, efficient, and reasonably priced active targeting strategy.

4.6.3.1 Mediators Improvement

Improving SAR values remains a challenging task, because the higher the SAR of the MNPs dispersion, the lower the dose to inject to the patient. Among the improvement routes, that which consists in the preparation of narrow size distribution MNPs is particularly pertinent for superparamagnetic mediators. Indeed, in conventional synthetic routes, the MNPs are far from being monodisperse in size, resulting in a distribution of relaxation times in the MNPs ensemble. As a consequence, for a specific frequency of the AC magnetic field, only a small fraction of MNPs heat efficiently (those whose relaxation times are fitting). Therefore, narrowing the size distribution could greatly improve the SAR values, because all the MNPs will heat efficiently at the same frequency.

However, very efficient mediators should not forget that the temperature in vivo must be tuned very precisely (see Sect. 4.6.1) because, on the one hand, heat conduction and energy adsorption are widely unknown in vivo, and on the other hand, local overheating may damage safe tissue. An original route could exploit the temperature dependence of magnetic properties of ferro-/ferrimagnets. So, it would consist in designing MNPs with a T_C adjusted to just above the temperature that should not be exceeded in vivo. In this way, should that temperature be reached, each nanoparticle mediator would function as its own fuse by losing its magnetic properties, and hence, also its heating capability. Such a strategy has already been developed for alloy seeds (macroscopic mediators) in order to prevent local tissue overheating and reduce the need for invasive thermometry. For MNPs, manganites ($La_{1-x}Sr_xMnO_3$) are promising materials whose T_C can be tuned in the range of 32–60 °C by varying the amount of Sr. The stabilization of temperature near T_C was observed for such MNPs when they were kept under AC magnetic fields [58]. Their synthesis in the form of narrow size distribution MNPs, their biocompatibility, and surface chemistry are currently under investigation by several groups.

Some of these constraints pull in opposite directions, for example, under physiological conditions, maximal SAR values are attained for superparamagnetic compounds, while in principle, only ferromagnetic or ferrimagnetic compounds allow self-controlled regulation. The aim here will thus be to find the best possible compromise. In addition, it does seem somewhat risky to depend only on

Brownian relaxation to reach sufficiently high values of the SAR from the therapeutic point of view, because unfortunately, once in the target tissues, or target cells, it is not obvious that the particles will be able to turn round owing to a high local viscosity or strong interactions with the cell membranes.

4.6.3.2 Physics of Magnetic Loss Phenomena

If the heating capacities of the mediators are to be improved, the models used up to now will need to be refined and extended, to increase their predictive power and to cover the whole range of sizes and magnetic behaviors. They must be systematically validated by experiment and the difficulties inherent in this approach will not be overcome without close collaboration between chemists and physicists, both in theory and practice. In particular, it is probably crucial to understand the influence of local clustering of MNPs in order to fully optimize the heating from real samples [48]. Moreover, SAR measurements by colorimetry must be performed in strict adiabatic conditions, that is, considering all the probable heat losses by convection, conduction, and radiation [18].

Lastly, modeling the temperature distribution in vivo remains a priority for determining the optimal ways of depositing energy, for example, continuously or in pulses.

4.6.3.3 Targeting Strategies and Limits

One of the last challenges will be to develop the intracellular hyperthermia route, which is based on *i.v.* administered stealth MNPs designed for selective uptake by tumor cells and which would be the optimal method allowing to selectively overheat tumor cells even in disseminated metastases in any region of the body. However, certain problems still exist as mentioned later.

The first one is the ligand-mediated targeting to improve the colloidal mediator uptake by cancer cells. Among several in vitro studies, a single group worked in vivo, with the use of ^{111}In-chimeric L6 monoclonal antibodies grafted onto dextran-coated iron oxide cores for human breast cancer in mice [59]. They reported a mean concentration of MNPs per gram of tumor of about 14 % of the injected dose, equivalent to around 0.315 mg per gram of tumor (315 mgmL^{-1}). This is an exceedingly small amount of MNPs being used to heat the tumor mass compared, for example, with the intratumoral concentrations obtained by the direct injection method of Jordan et al., which were greater than 10 mgmL^{-1} of tumor.

The second one is the monitoring of the tissue distribution prior to the heating sequence. MRI appears to be the most suited method, and therefore, a great interest exists to investigate a unique and versatile magnetic device that will be able to reveal tumors and metastases and treat them by hyperthermia.

The last one concerns the debate about the expected higher efficacy of intracellular thermotherapy, which is obtained with magnetic particles internalized

within cells, with regard to extracellular thermotherapy. According to a theoretical model, it would seem that there is no thermotherapeutic effect on the nanoscale (the scale of the MNPs) or the microscale (the scale of the cells). In fact, thermotherapy operates on the millimeter scale (the scale of the tumor), since the thermal insulation behavior of the cell membrane is negligible [60]. Any difference that may be observed between intracellular and extracellular thermotherapy would thus appear to be due to a mechanical effect of rotation or vibration of the particles in the cell.

Extending this work to highlight the difficulties of using currently available MNPs to heat anything smaller than a 10 mm diameter tumor, an excellent analysis of the various opportunities and limitations was recently published [61]. The issue is essentially one of heat loss into the surrounding tissue. If one wishes to generate and sustain a large temperature imbalance within a tumor, the heat flow into that tumor has to be so large as to overcome the heat flow out. Roughly speaking, the bigger the tumor, the smaller the surface area to volume ratio, the less important the outward heat flow, and the easier it is to heat. Following this argument, the authors concluded that the MNPs SAR must be unrealistically high (certainly several orders of magnitude greater than the best currently reported) to heat a 3 mm cluster of cells, even with concentrations of iron in the cellular mass of 10–50 mgmL^{-1}. These figures are relevant given that $\sim$3 mm is the size of a subclinical metastasis that is undetectable by normal imaging techniques, and 10 mgmL^{-1} is substantially more than was used in vivo by DeNardo et al., but in the realm of that used by Jordan et al. The situation becomes even worse if the aim is to heat individual cells [48].

4.7 Conclusion

In this chapter, recent advances in biomedical applications of MNPs are reviewed. Iron oxide MNPs are now routinely used as contrast agents in MRI and very next clinical applications are expected in the field of cancer thermal treatment. These devices will be nanomaterials of higher and higher added value because they are expected to be multifunctional, smart, and versatile. Therefore, their chemical composition shall be more and more hybrid combining inorganic, organic, and biologic components. Nevertheless, optimization efforts remain for improving the repeatability of surface functionalization, diagnostic or therapeutic efficacy, biodistribution, and in vivo stability and safety. But the readers shall be convinced that targeting remains the main challenge, for which concentrated research efforts are still required.

Such developments of medicine-directed nanotechnology are probably among the best examples where physicians, pharmacologists, biologists, chemists, and physicists are working together. In this day, when the public opinion worries rightly about the possible nanotechnology consequences on mankind and its environment, it is important to mention that the single aim of a large number of these research efforts on nanoparticles is the humanity survival and comfort.

References

1. Häfeli U (2007) In Magnetism in Medicine: A Handbook. Andrä W, Nowak H (eds). Wiley, Weinheim pp 3–25
2. Corot C, Robert P, Idée JM, Port M (2006) Adv Drug Deliv Rev 58:1471–1504
3. Moghimi SM, Szebeni J (2003) Prog Lipid Res 42:463–478
4. Monfardini C, Veronese FM (1998) Bioconjug Chem 9:418–450
5. O'Handley RC (2000) Modern magnetic materials: principles and applications. Wiley, New York
6. Spaldin N (2003) Magnetic materials: fundamentals and device applications. Cambridge University Press, Cambridge
7. Pankhurst QA, Connolly J, Jones SK, Dobson JJ (2003) Phys D Appl Phys 36:R167–R181
8. Jeong U, Teng X, Wang Y, Yang H, Xia Y (2007) Adv Mater 19:33–60
9. Goya GF, Grazú V, Ibarra MR (2008) Curr Nanosci 4:1–16
10. Néel L (1949) Ann Géophys 5:99–136
11. Brown WF (1963) Jr Phys Rev 130:1677–1686
12. Lu JJ, Deng HY, Huang HL (2000) J Magn Magn Mater 209:37–41
13. Hergt R, Dutz S, Müller R, Zeisberger MJ (2006) Phys Condens Matter 18:S2919–S2934
14. Rosensweig REJ (2002) Magn Magn Mater 201:370–374
15. Kallumadil M, Tada M, Nakagawa T, Masanori A, Southern P, Pankhurst QA (2009) J Magn Magn Mater 321:1509–1513
16. Schmidt AM (2007) Colloid Polym Sci 285:953–966
17. Hergt R, Andrä W (2007) In magnetism in medicine: a handbook. In: Andrä W, Nowak H (eds) Wiley, Berlin pp 550–570
18. Natividad E, Castro M, Mediano A (2008) Appl Phys Lett 92:093116
19. Natividad E, Castro M, Mediano AJ (2009) Magn Magn Mater 321:1497–500
20. Kaman O, Veverka P, Jirák Z, Maryško M, Knížek K, Veverka M, Kašpar P, Burian M, Šepelák V, Pollert EJ (2011) Nanopart Res 13:1237–1252
21. Lu AH, Salabas EL, Schüth F (2007) Angew Chem Int Ed 46:1224–1244
22. Duran JDG, Arias JL, Gallardo V, Delgado AVJ (2008) Pharm Sci 97:2948–2983
23. Roca AG, Costo R, Rebolledo AF, Veintemillas-Verdaguer S, Tartaj P, Gonzalez-Carreno T, Morales MP, Serna CJJ (2009) Phys D Appl Phys 42:224002–224011
24. Dave SR, Gao X (2009) Wiley Interdiscip Rev Nanomed Nanobiotechnol 1:583–609
25. Di Marco M, Sadun C, Port M, Guilbert I, Couvreur P, Dubernet C (2007) Int J Nanomed 2:609–622
26. Lin MM, Kim DK, El Haj AJ, Dobson J (2008) IEEE Trans Nanobiosci 7:298–305
27. Majewski P, Thierry B (2007) Crit Rev Solid State Mater Sci 32:203–215
28. Jech TJ, Odenbach S, Odenbach S (2003) Ferrofluids: magnetically controllable fluids and their applications. Springer, New York
29. Massart R (1981) IEEE Trans Magn 17:1247–1248
30. Neuberger T, Schöpf B, Hofmann H, Hofmann M, von Rechenberg BJ (2005) Magn Magn Mater 293:483–496
31. Shubayev VI, Pisanic TR, Jin S (2009) Adv Drug Deliv Rev 61:467–477
32. Moghimi SM, Hunter AC, Murray JC (2001) Pharmacol Rev 53:283–318
33. Vonarbourg A, Passirani C, Saulnier P, Benoit JP (2006) Biomaterials 27:4356–4373
34. Arruebo M, Valladares M, Gonzalez-Fernandez A (2009) J Nanomater 24; article ID 439389
35. Peng XH, Qian X, Mao H et al (2008) Int J Nanomed 3:311–321
36. Thierry B (2009) Curr Drug Deliv 6:391–403
37. Stella B, Arpicco S, Peracchia MT et al (2000) J Pharm Sci 89:1452–1464
38. Brown MA, Semelka RC (2003) MRI: basic principles and applications, 3rd edn. Wiley, New York
39. Weinmann HJ, Ebert W, Misselwitz B, Schmitt-Willich H (2003) Eur J Radiol 46:33–44
40. Bonnemain BJ (1998) Drug Target 6:167–174

41. Wallis F, Gilbert FJJR (1999) Coll Surg Edinb 44:117–125
42. Harisinghani MG, Barentsz J, Hahn PF et al (2003) New Engl J Med 348:2491–2499
43. Weinstein JS, Varallyay CG, Dosa E et al (2010) J Cereb Blood Flow Metab 30:15–35
44. Bulte JWM, Kraitchman DL (2004) NMR Biomed 17:484–499
45. McCarthy JR, Weissleder R (2008) Adv Drug Deliv Rev 60:1241–1251
46. Högemann D, Josephson L, Weissleder R, Basilion JP (2000) Bioconjug Chem 11:941–946
47. Mornet S, Vasseur S, Grasset F, Duguet EJ (2004) Mater. Chem. 14:2161–2175
48. Pankhurst QA, Thanh NKT, Jones SK, Dobson JJ (2009) Phys D Appl Phys 42:224001–224015
49. Jang JT, Nah H, Lee JH, Moon SH, Kim MG, Cheon J (2009) Angew Chem Int Ed 48:1234–1238
50. Sneed P K, Stea B (1996) In thermoradiotherapy and thermochemotherapy. In: Seegenschmiedt MH, Fessenden P, Vernon CC (eds) Springer, Berlin, vol 2, pp 159–173
51. Luchetti F, Mannello F, Canonico B et al (2004) Apoptosis 9:635–648
52. Gilchrist RK, Medal R, Shorey WD et al (1957) Ann Surg 146:596–606
53. Jordan A, Scholz R, Wust P et al (1997) Int J Hyperther 13:587–605
54. MagForce nanotechnologies AG, www.Magforce.de
55. Johannsen M, Gneveckow U, Thiesen B et al (2007) Eur Urol 52:1653–1662
56. Johannsen M, Gneveckow U, Eckelt L et al (2005) Int J Hyperther 21:637–647
57. Maier-Hauff K, Rothe R, Scholz R et al (2007) J Neurooncol 81:53–60
58. Pollert E, Knizek K, Marysko M, Kaspar P, Vasseur S, Duguet EJ (2007) Magn Magn Mater 316:122–125
59. DeNardo SJ, DeNardo GL, Natarajan A et al (2007) J Nucl Med 48:437–444
60. Rabin Y (2002) Int J Hyperther 18:194–202
61. Hergt R, Dutz SJ (2007) Magn Magn Mater 311:187–192